Springer Ser Chem Sens Biosens (2007) 5: 449–479
DOI 10.1007/5346_035

Published online: 8 July 2006

Resonant Acoustic Profiling (RAP™) and Rupture Event Scanning (REVS™)

Matthew A. Cooper

Akubio Ltd., Cambridge Science Park, Cambridge CB4 0GJ, UK
mcooper@akubio.com

Abstract Following the release of widely available commercial instruments in the 1990s, researchers have driven the development of biosensor-based methods for profiling and screening of small molecule and proteinaceous therapeutic drug candidates. Medicinal chemists have in turn demanded faster and more accurate assays for characterisation of drug candidate interactions with target receptors, serum proteins and side-effect profiling receptors. In response to this challenge, Akubio Ltd. (Cambridge, UK) has been developing an advanced label-free detection platform, resonant acoustic profiling (RAP™). This evolution of the basic QCM approach has the potential to change the way assays are performed and to generate novel information on molecular interactions. Key attributes covered in this chapter include the ability to multiplex to high numbers of resonators, the addition of robust interfacial surface chemistries, fully automated sample handling and sample processing, disposable microfluidic cassettes with submicrolitre dead volumes, and more sensitive detection electronics.

Akubio has also developed a sensitive and economical method to directly detect particulate analytes. The technique, which we term rupture event scanning (REVS™), is based on control of the amplitude of oscillation of an acoustic wave device on which the analytes have been captured. In this chapter, example applications of RAP™ for proteins

and small molecules and REVS™ for virus detection are presented. The physical forces involved in the processes are also discussed.

Keywords Surface chemistry · Microfluidics · Affinity · Kinetics · Force

Abbreviations

BAW	Bulk acoustic wave
BSA	Bovine serum albumin
EDC	1-Ethyl-3-[3-dimethylaminopropyl]carbodiimide hydrochloride
GDH	Glucose dehydrogenase
IL-1β	Interleukin 1-beta
ITC	Isothermal titration calorimetry
Ms IgG	Mouse immunoglobin type G
NHS	*N*-Hydroxysuccinimide
PBS	Dulbecco's modified phosphate buffered saline
QCM	Quartz crystal microbalance
QCRS	Quartz crystal resonance sensing
RaM-FC	Rabbit anti-mouse (Fc-specific) immunoglobin
RAP™	Resonant acoustic profiling
REVS™	Rupture event scanning
SPR	Surface plasmon resonance
Tween-20	Polyoxyethylenesorbitan monolaurate

1 Resonant Acoustic Profiling

1.1 Benefits of Label-Free Technology

Over the past two decades the benefits of label-free analyses have begun to make an impact on their use as mainstream research tools in many laboratories [1, 2]. Label-free biosensors do not require the use of detection labels (fluorescent, radio or colorimetric) to facilitate measurements. Detailed information on an interaction can be obtained during analysis whilst minimising sample processing requirements and assay run times [3]. Unlike label- and reporter-based technologies that simply confirm the presence of the detector molecule, label-free techniques can provide direct information on analyte binding to target molecules, typically in the form of mass addition or depletion from the surface of the sensor substrate [4]. However, these technologies have failed to gain widespread acceptance due to technical constraints, low throughput, high user expertise requirements and cost. Whilst they can be powerful tools in the hands of a skilled user evaluating purified samples, they are not readily adapted to everyday laboratory use where simple-to-understand results on high numbers of samples are the norm.

Resonant acoustic profiling (RAP™) from Akubio (Cambridge, UK) provides researchers with the ability to perform accurate real-time, label-free characterisations on both purified and crude samples in an easy to use format. RAP™, which is based on piezoelectric quartz crystal technology, measures the build-up of molecules on the surface of an oscillating crystal and provides real-time binding information on the binding interactions. The piezoelectric effect was first noted by the Curie brothers in 1880 [5]. Today, acoustic devices based on quartz crystal resonators are found in electronic devices such as watches, computers and televisions, with over a billion units mass-produced each year. Application to biological samples became possible when suitable oscillator circuits for operation in liquids were developed [6, 7]. As molecules interact with immobilised receptors on the surface of a quartz crystal, there is a concomitant modulation of the acoustic resonance of the crystal. This, in turn, results in modulated electrical signal that can be analysed using standard digital signal processing techniques [8]. The signal indicates not only the presence of the analyte but also the specificity and affinity for a surface-bound receptor. When combined with a flow-based microfluidic chip, kinetic parameters and complex half-lives can also be quantified. Additional evaluations of the viscoelastic properties of binding events, through analysis of parameters such as motional resistance, may provide unique data relevant to structural properties and confirmation changes associated with molecular interaction [9]. The simultaneous measurement of these parameters creates an acoustic profile of a molecular interaction, giving a high level of information about a binding event on a routine basis.

1.2 Literature Trends

There has been continued growth in the number of publications referencing the term "quartz crystal microbalance" or "QCM" in which a thickness shear mode bulk acoustic wave resonator is used to probe biological and chemical interactions in life sciences research. As alluded by other contributors to this volume, the term "microbalance" is not strictly accurate: many examples of non-gravimetric responses of acoustic wave devices to analyte binding have been reported in the literature [10–15]. Nevertheless, the terms QCM, QCRS ("quartz crystal resonance sensing") and BAW ("bulk acoustic wave") can be cross-referenced with terms such as "biosensor" and "analyte" to ensure that the vast majority of publications in the field are captured. Following this approach, it is immediately obvious that the number of publications that involve the use of QCM has increased rapidly since the mid-1980s (Fig. 1a). Many of the separate hardware components that make up an acoustic biosensor are commercially available from a number of electronics companies: a lock-in amplifier, a frequency synthesiser, a power supply and a quartz crystal holder. This provides a low barrier to entry for the academic or industrial re-

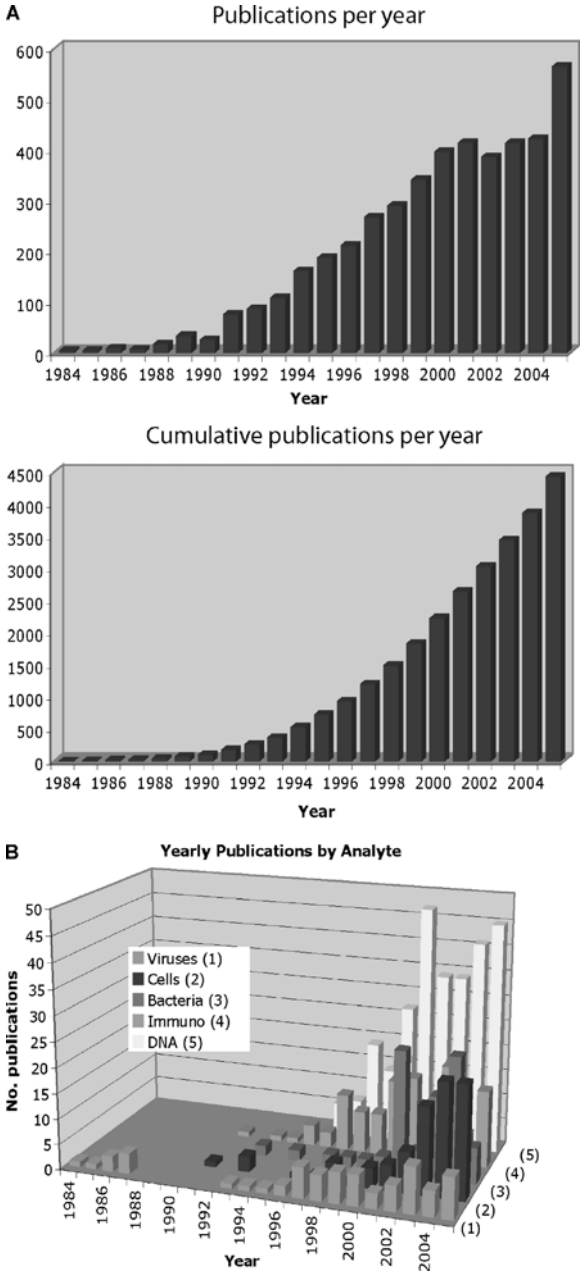

Fig. 1 QCM publications. **A** Yearly cumulative number of publications found using an ISI Web of SCIENCE® search for the term "quartz crystal microbalance" in the title, keyword or abstract. **B** Yearly number of publications found using an ISI Web of SCIENCE® search for the term "quartz crystal microbalance" cross referenced using the terms "DNA", "immunoassay", "bacteria", "cell" or "virus"

Table 1 Published limits of detection for selected clinically relevant immunoassays

Analyte	Matrix	Sensitivity	Refs.
African swine fever virus	Serum	Ag 1 $\mu g\,mL^{-1}$ IgG 0.2 $\mu g\,mL^{-1}$	Uttenthaler 1998 [23]
Anti-*T. gondii* IgG	Blood, serum	1 : 5500	Wang et al. 2004 [24]
Anti-*T. pallidum* IgG	Serum	75–900 mIU	Aizawa et al. 2001 [25]
Complement C4	Serum	0.1–10 $\mu g\,mL^{-}1$	Hu et al. 1998 [26]
C-reactive protein	Serum	10–70 $\mu g\,mL^{-1}$	Aizawa et al. 2001 [16]
Der p (house dust mite) IgE	Serum	0.15 IU mL^{-1}	Su et al. 2000 [27]
Fibrinogen	Serum	10 $\mu g\,mL^{-1}$	Aizawa et al. 2003 [28]
Niacinamide	Serum, urine	1 nM	Long et al. 2001 [29]
Total IgE	Serum	5–300 IU mL^{-1}	Su et al. 1999 [30]
Transferrin	Serum	160 ng mL^{-1}	Wu et al. 2000 [21]

Table 2 Published limits of detection for selected clinically relevant bacteria

Analyte	Matrix	Sensitivity (cfu/mL)	Refs.
S. epidermidis	Growth medium	100	Bao et al. 1996 [31]
L. monocytogenes	Milk	250 000	Minunni et al. 1996 [32]
C. trachomatis	Urine	260 ng mL^{-1}	BenDov et al. 1997 [17]
S. typhimurium	Buffer	530 000	Ye et al. 1997 [33]
S. typhimurium	Growth medium	990 000	Park et al. 1998 [34]
S. typhimurium	Milk	3 200 000	Park et al. 2000 [35]
S. paratyphi A	Growth medium	170	Fung et al. 2001 [36]
T. pallidum	Serum	10–600 TU	Aizawa et al. 2001 [37]

searcher, when compared to the expense and expertise required to assemble an optical platform (which usually require sophisticated CCD cameras, processing software, optical filters, optical interfaces, lasers etc.). As a result, from 1990 to 2000 the number of publications involving QCM has grown semi-exponentially; the rate of growth slowing slightly from 2000 to 2004 (Fig. 1a).

This period has also seen an increase in the number of publications that describe the detection and quantification of clinically relevant analytes [16–22], (Fig. 1b). Published limits of direct detection (LOD) for analytes present in serum, blood or urine are typically in the range 0.1–10 $\mu\,gL^{-1}$ (1). Whilst these LODs can meet, or surpass the clinically relevant LODs for many analytes, there are numerous other examples where $pgmL^{-1}$ or even $fgmL^{-1}$ detection sensitivity is required for accurate diagnosis. However, it is notable

that these data were generated on "home built" QCM systems often using very basic receptor attachment chemistries.

There has been a steady growth in the number of published papers describing detection of clinically relevant bacteria [36, 38–42] (Table 2 and Fig. 1b) and, in the last 5 years, there has been a rapid growth in the number of publications using acoustic biosensors to analyse mammalian cells [43–51]. In the latter application, a variety of cell types have been immobilised on quartz resonators coated with appropriate attachment chemistries. Here the cell forms an active part of the biological transducer component of the sensor, as bulk viscoelastic changes in the cell are also detected via the quartz resonator. This approach has been employed to monitor interactions between cells and the adherent surface, as well as the cellular response to a variety of exogenous stimuli. Both the magnitude and kinetics of the response can be followed, as detection occurs in real-time and does not require fluorescent, chemiluminscent, quantum dot or other reporter labels.

The number of publications using acoustic sensing to measure hybridisation of nucleotides, particularly single-stranded DNA (ssDNA), has grown dramatically since 1996 (Fig. 1b). Recent work has shown that it is possible to sensitively and specifically detect genetically modified organisms and even single base-pair mismatches from PCR-amplified contaminated foodstuffs and pooled patient sera [52–56]. The ability to probe for pathogen nucleic acid, pathogen antigen and pathogen-specific host antibodies provides extra levels of assay redundancy, giving greater confidence in the results. In time this capacity should enable the development of very robust and precise pathogen detection systems that give information on pathogen copy number, antigen level and immunological host response.

1.3 RAP♦*id*™ System

The breadth of application areas described above is significant, with numerous published papers that describe the detection of nearly all classes of clinically relevant analytes. However, it is surprising that these data have almost exclusively been generated using "home built" QCM systems, often with insufficient attention to surface chemistry and assay reproducibility. A widely available and robust acoustic detection system that can generate reproducible data for the above classes of analytes could be of great benefit to life sciences research, clinical diagnostics, environmental sensing and homeland defence communities. In response to this challenge we are developing RAP™ systems that incorporate a number of key technical advances compared to the prior art. We have produced high frequency resonators that possess high merit or *Q* factors (a measure of the piezoelectric device's ability to convert electrical energy into kinetic energy). This increases the detection sensitivity [57] and also improves assay reproducibility. These resonators incorporate a parallel

reference control, which enables analyte to be passed simultaneously over both "active" and "control" receptors. Real-time subtraction of control data from active data further improves the robustness of the assay.

There have been major advances in the field of microfluidics that enable sophisticated devices to be developed, tested and ultimately released to the market over a much shorter time scale than was possible a decade earlier. As quartz is a piezoelectric material, it is highly sensitive to flexural, shear and pressure changes. These artefacts are undesirable in a system designed to measure a specific response to analyte. To address this potential problem, we have combined a proprietary stress-free mounting system for the quartz crystal with a microfluidic lateral flow device with a dead volume of less than one microlitre. This ensures that the detector response is sensitive principally to analyte binding. It also enables a relatively small (< 30 microlitre) volume of liquid to be delivered and removed from the resonant sensing area rapidly and efficiently with minimal sample dispersion or sample cross-contamination (Fig. 2). RAP™ experiments described in this paper were conducted using manually operated or automated two- and four-channel instruments (Akubio, Cambridge, UK). The instruments applied the principles of QCM, in that a high frequency voltage was applied to a piezoelectric crystal to induce the crystal to oscillate, and its resonance frequency was monitored in real time. The two-channel instruments comprised a pair of oscillating crystal sensors mounted in parallel microfluidic flow cells, allowing sample to be flowed across two surfaces simultaneously. As sample is flowed across "control" and "active" sensors, binding to the "active" sensor is measured as a reduction in the oscillation frequency, with the "control" sensor acting as a subtractive sample reference. The RAP™ instruments were fitted with a thermally stable sensor mounting block providing temperature control, and with microfluidic and electrical connections to the pair of piezoelectric sensors. Buffer flow was maintained with two sy-

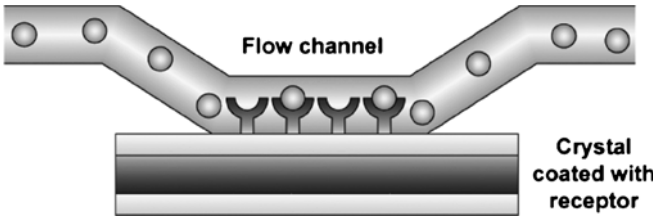

Fig. 2 Microfluidic biosensor chip. Pictorial representation of a piezoelectric bioassay: a piezoelectric acoustic wave device (such as a quartz crystal resonator) is coated with a selective, passivating layer to which an analyte-specific receptor can be immobilised. Liquid containing the analyte of interest is then passed across the surface using appropriate microfluidics, which results in selective capture of the analyte. This additional bound material in turn modulates resonance of the acoustic wave device, which is transformed into an electrical signal due to the piezoelectric effect

ringe pumps (Tecan UK, Reading, UK) under software control (Akubio). Microfluidics comprised separate flow paths to individual flow cells, combined with a common flow path split to address both flow cells simultaneously. Interchange between the different flow paths was either by manually or electronically operated valves (Akubio). Sensors comprised standard gold-coated quartz wafers, with a carboxylic acid-terminated linker layer coating to provide a surface for protein immobilisation, mounted in an acrylic cassette (Akubio).

1.4 Linker Chemistry

The interface between the biosensor surface and the chemical or biological systems to be studied is a vital component of all surface-sensitive sensor systems. Receptors must be attached to some form of solid support whilst retaining their native conformation and binding activity. This attachment must be stable over the course of a binding assay and, in addition, sufficient binding sites must be presented to the solution phase to interact with the analyte. Most importantly, the support must be resistant to non-specific binding of the sample matrix, which could mask the analyte-binding signal. Many receptor-coupling strategies utilise a chemical linker layer between the sensor base interface (e.g. a gold layer) and the biological component to achieve these ends. The termini of these molecules can be derivatised with molecules that possess suitable chemical reactivity for receptor capture (e.g. -epoxy, -carboxyl, -amino, -biotinyl, -nitrilotriacetic acid) [58–60]. The receptor is normally immobilised on the surface, and the binding partner (analyte) is allowed to bind to this surface from free solution. However, it is also possible to configure solution competition assays in which the analyte is immobilised on the surface and competes with solution-phase analyte for receptor.

Selection of the correct coupling chemistry requires careful consideration of: (a) the resultant orientation of receptor, (b) its local environment on the surface, (c) the stability of the linkage under the conditions used to regenerate the surface, and (d) possible effects of the coupling chemistry on components of the binding interaction. We have employed a carboxylic acid-terminating linker layer together with carbodiimide-mediated amine coupling (e.g. to surface lysine residues or *N*-terminal residues on a proteinaceous receptor). If immobilisation is performed at low pH, the amine terminus of the receptor is likely to be more reactive than the gamma-amino group of any lysine residues, in which case amine coupling can give rise to more ordered surface orientation. A control receptor (e.g. BSA or non-specific IgG) can be coupled to a control resonator surface, and the active receptor is coupled to an adjacent resonator surface. Note that it is also possible to couple sulfhydryl-containing receptors or thiolated oligonucleotide probes using chemically selective cross-linking reagents such as pyridinyldithioethanamine (PDEA)

or 3-(2-pyridinyldithio)propionic acid *N*-hydroxysuccinimide ester (SPDP) to achieve an even higher degree of receptor orientation homology.

1.5 RAP™ Assays

After the immobilisation of "control" and "active" receptors, the resultant "sensor chip" can then be stored for future use, or used directly after receptor immobilisation. In a typical RAP™ assay (Fig. 3) at $t = 0$ s, buffer was contacted with the receptor via the microfluidic device. At $t = 60$ s a solution of analyte (in this case mouse IgG) in the running buffer was passed over the active surface (rabbit anti-mouse-Fc) and the control surface (mouse IgG). As the analyte bound to the active receptor, the additional mass and viscoelastic load on the resonator resulted in a change in the resonance signal (depicted here as a negative change in series resonance).

For this simple bimolecular association, $A + B = AB$, the process was assumed to be pseudo first order with no interaction between separate receptor molecules. The dissociation rate is derived from:

$$R_t = R_{t_0} e^{-k_d(t-t_0)}, \tag{1}$$

where R_t is the response at time t, R_{t_0} is the response at time t_0 and k_d is the dissociation rate constant. The association rate constant can be derived using

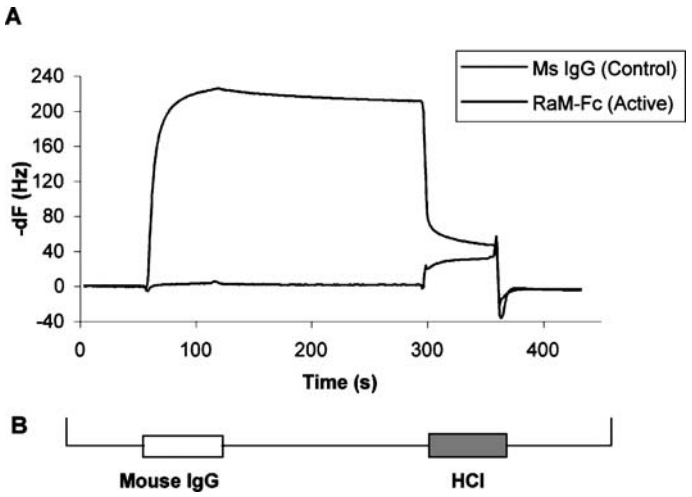

Fig. 3 Typical RAP™ assay with binding and regeneration. **A** Binding of Ms IgG to RaM-Fc active and Ms IgG control sensor surfaces. *Top line* indicates the frequency response generated by binding of Ms IgG to RaM-Fc and the *bottom line* indicates the frequency response generated by minimal binding to the control Ms IgG surface. **B** Schematic representation of sample and regeneration solution injections

the equation:

$$R_t = \frac{k_a\ CR_{max}\left(1 - e^{-(k_a\ C + k_d)t}\right)}{k_a\ C + k_d}, \tag{2}$$

where R_{max} is the maximum response (proportional to the amount of immobilised ligand), C is the concentration of analyte in solution and k_a is the association rate constant. Analysis of the association phase of the binding curve gives directly the observed association rate (k_{obs}). If the concentration of the analyte is known, then the association rate constant of the interaction (k_a) can be determined. Conversely, if the kinetic parameters for an interaction are known (i.e. fixed for a given receptor–analyte interaction), it is possible to derive the active concentration of an analyte in a sample.

Affinities were then calculated from the ratio of k_a/k_d and also from analysis of equilibrium binding levels at varying analyte concentration. By measuring the signal attained at equilibrium as a function of analyte concentration, affinities can be determined from a Scatchard analysis using the equation:

$$\frac{R_{eq}}{C} = K_a R_{max} - K_a R_{eq}, \tag{3}$$

where R_{eq} is the response at equilibrium and K_a is the association constant ($1/K_d$). A plot of R_{eq}/C versus R_{eq} has a slope of $-K_a$.

In the example shown in Fig. 3, at $t = 240$ s the mouse IgG solution was replaced by buffer and the receptor–analyte complex was allowed to dissociate. Analysis of this data can gave the dissociation rate constant (k_d) for the interaction. Many complexes in biology have considerable half-lives, thus a pulse of a regeneration solution (in this case an acid wash followed by a basic wash) was used at $t = 240$ s and $t = 360$ s to disrupt binding and regenerate the free receptor. The entire binding cycle can be repeated many times at varying concentrations of analyte to generate a robust data set for global fitting to an appropriate binding algorithm. The affinity of the interaction was then calculated from the ratio of the rate constants ($K_d = 1/K_a = k_d/k_a$) and confirmed by a non-linear fitting of the response at equilibrium versus varying concentration of analyte.

1.6 Myoglobin

Myoglobin is a 17 kDa cytoplasmic protein found in muscle cells that binds and stores oxygen. Normal levels of myoglobin in blood are very low ($< 100\ ng\ mL^{-1}$). Following muscle damage (e.g. cardiac ischemia), myoglobin is released into the blood and can rise to $> 1000\ ng\ mL^{-1}$ immediately after a myocardial infarction, and can remain high ($\sim 500\ ng\ mL^{-1}$) for some time afterwards. Myoglobin detection in blood is therefore a good diagnostic indicator of preceding and ongoing cardiac disease and damage [61]. We used

a mouse anti-myoglobin antibody, previously captured onto a rabbit anti-mouse-Fc (RaM-Fc) surface to measure binding of varying concentrations of human recombinant myoglobin in real time (Fig. 4a).

Varying concentration of myoglobin in the sample would give varying response levels at equilibrium, which would enable generation of a standard curve for analyte concentration. However, it can be seen from Fig. 4a, that at lower concentrations of myoglobin considerable contact time would be required to reach an equilibrium level. In addition, in a "real world" diagnostic application the sensor is likely to be used only once, and the level of receptor activity may vary upon shipping and storage, which would result in variable equilibrium binding levels. Hence, analyte concentration can be more accu-

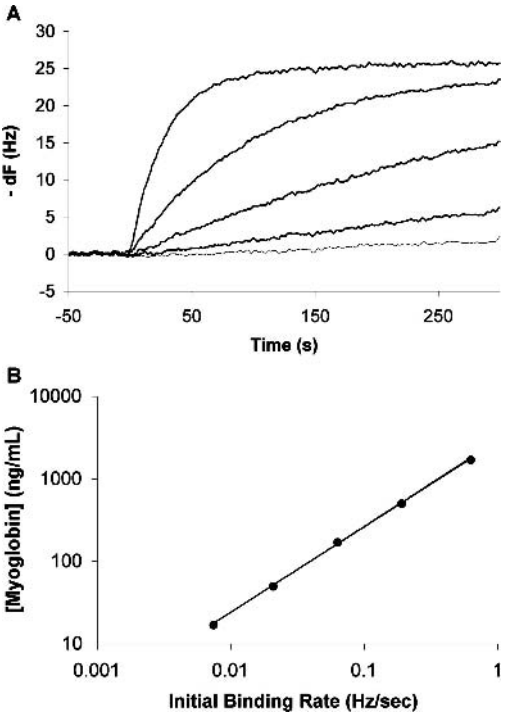

Fig. 4 Myoglobin concentration assay. **A** Binding of recombinant human myoglobin to mouse anti-myoglobin antibody, previously captured onto a RaM-Fc surface. Binding curves for five different standard myoglobin concentrations (equivalent to 100, 30, 10, 3 and 1 nmol L^{-1}) are shown overlaid and synchronised to the start of each myoglobin injection. Correction for signal drift due to the off-rate of the captured antimyoglobin antibody was performed by subtraction of the response from injection of buffer only. **B** Myoglobin concentration–response calibration curve, generated by plotting the initial binding rate for the set of standard concentrations. Estimates of myoglobin concentration in unknown samples were calculated by linear interpolation from the calibration curve with an accuracy of 0.5–15% over the concentration range tested

rately and rapidly determined by analysing the rate of binding of myoglobin to the antibody, and comparing the measured observed association rate with a data set calibrated to analyte concentration (Fig. 4b). This enabled the concentration of myoglobin in the sample to be determined in under 6 min.

1.7 Interleukin 1-Beta

Members of the interleukin-1 (IL-1) family have clear therapeutic and diagnostic potential: the IL-1 agonists, IL-1α and IL-1β, are induced by central nervous system injury, whilst peripheral or central administration of the IL-1

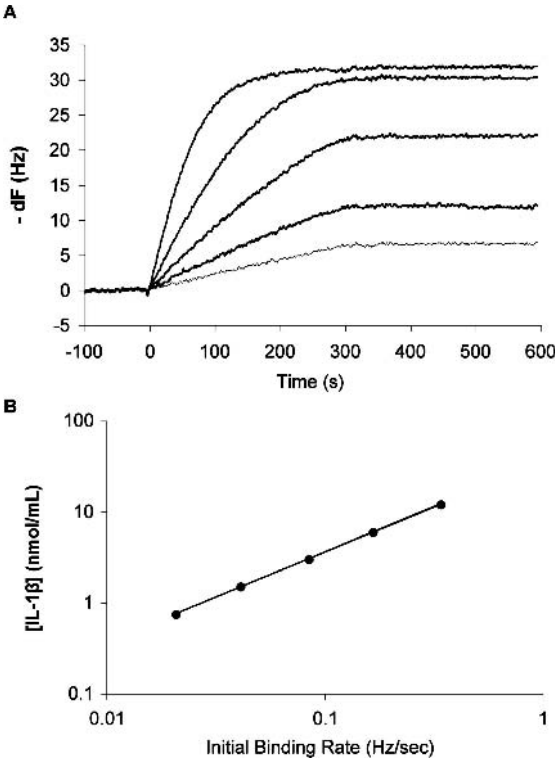

Fig. 5 Interleukin 1-beta concentration assay. **A** Binding of human IL-1β to mouse anti-IL-1β antibody, previously captured onto a RaM-Fc surface. Binding curves for five different IL-1β concentrations are shown overlaid, synchronised to the start of each IL-1β injection. Data have been normalised by subtraction of the response to injection of buffer alone, to correct for the off-rate of the captured anti-IL-1β antibody. **B** IL-1β concentration–response calibration curve. The initial binding rate for each IL-1β concentration was calculated as for the myoglobin concentration–response calibration curve (Fig. 4)

antagonist, IL-1ra, reduces the extent of the damage by more than 50%. The mechanism of action of these cytokines is the subject of intense research [62]. IL-1β is a 17.3 kDa protein that is found in serum, mucosa and in pleural effusions of different etiologies. It has been suggested as a diagnostic marker in the differential diagnosis of several pleural diseases [63]. It has also been found at consistently raised levels in normal appearing mucosa from patients with Crohn's disease, potentially providing evidence for a sustained immune stimulation in Crohn's disease in the absence of patent inflammation [64]. We used a mouse anti-IL-1β antibody, previously captured onto a RaM-Fc surface to bind to varying concentrations of human IL-1β (Fig. 5a).

As in the case for myoglobin, analyte concentration was more accurately and rapidly determined by analysing the rate of binding of IL-1β to the antibody, and comparing the measured observed association rate with a data set calibrated to analyte concentration (Fig. 5b). This also enabled the concentration of IL-1β in the sample to be determined in under 6 min.

1.8 Glucose Dehydrogenase

Glucose dehydrogenase (GDH) is a key initial enzyme in the energy production process that uses nucleotide cofactors to "activate" monosaccharide sugars as a prelude to their subsequent breakdown into pyruvate to enter the Krebs cycle. Nicotinamide adenine dinucleotide phosphate ($NADP^+$, 765 Da) is the preferred cofactor, nicotinamide adenine dinucleotide (NAD^+, 663 Da) will act as a lower activity cofactor, and flavine adenine dinucleotide (FAD, 830 Da) will not bind nor act as cofactor. Preferred monosaccharide substrates for the enzyme are glucose and galactose (180 Da). Other monosaccharides (e.g. fructose, 180 Da) and disaccharides (e.g. maltose, sucrose, 342 Da) cannot act as substrates.

Glucose dehydrogenase was coupled to a carboxylic acid terminating linker layer using standard carbodiimide amine coupling as described earlier. BSA was coupled in a similar manner to a second sensor surface to be used as a passive control. $NADP^+$, NAD^+ and FAD were then independently serially diluted and injected across the GDH "active" and BSA "control" surfaces for 1 min. The complexes were then allowed to dissociate for 1 min until pre-binding baseline levels were attained (Fig. 6).

From simple visual inspection of the magnitude of the binding response of the different cofactors, a rapid estimate of ranking affinity can be made: $NADP^+ > NAD^+ >$ FAD. The equilibrium binding constant, K_D, for $NADP^+$ binding to GDH, was calculated from analysis of equilibrium binding levels resulting from injection of threefold dilutions of $NADP^+$. The average response during the "plateau" phase of binding was plotted against $NADP^+$ concentration, and these data were fitted to a sigmoidal single site binding model to give a K_D of 2.8 mM. This demonstrates that RAP™ can be applied

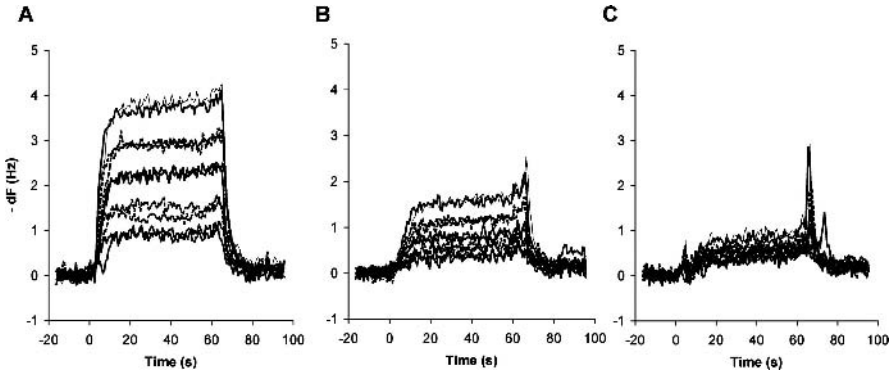

Fig. 6 Enzyme cofactor screening. Binding of preferred substrate, poor substrate, and non-preferred adenine-nucleotide cofactors to the metabolic enzyme GDH. **A** NADP (765 Da, preferred substrate) binding shows a clear equilibrium concentration–response relationship. **B** NAD (663 Da, metabolite) shows a lower equilibrium binding level, and compressed concentration–response relationship. **C** FAD (830 Da, non-preferred substrate) shows very low levels of equilibrium binding

to the accurate determination of cofactor affinities for an enzyme in real time in less than 20 min.

1.9 Automation

Scheduled for full commercial launch in 2006, the first instrument from Akubio, employing resonant acoustic profiling technology, the RAP♦*id*-4 (Fig. 7), integrates the RAP™ detection technology with a continuous flow microfluidic liquid delivery system, a thermal control unit, and automated sample

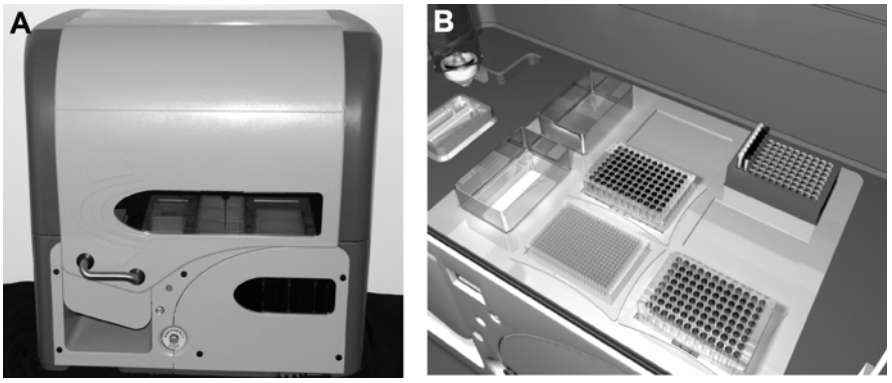

Fig. 7 RAP♦*id*-4™ system (*left*) and view of the sample rack and injection interface (*right*)

handling. Fitted with four individually addressable sensors, the instrumentation can provide specificity, affinity and kinetic characterisations for more than 200 samples per day. The system is capable of working in a variety of different solvents and in complex biological mixtures. For example, interactions can be studied in solutions containing up to 10% DMSO, in cell lysates, and in cell culture media.

1.10 Challenges for Label-Free Technologies

All optical label-free detection methods ultimately measure changes in dielectric constant or refractive index of a solution in close proximity to the surface of the sensor substrate. Whilst they are powerful techniques under extremely well controlled conditions, the advantages are often minimised when trying to apply these methods in routine analysis procedures. As optical methods rely on proximity-based detection, any analyte that is within the evanescent sensing field (typically 300 nm for most SPR devices) is detected as "bound". This is the case whether it physically bound to the receptor or simply in close proximity to the surface of the sensor. In contrast, RAP™ measures only those materials that are acoustically coupled to the sensor surface, i.e. binding-based detection rather than proximity-based detection. The process of measuring refractive index changes with optical methods to infer mass changes imparts a number of other intrinsic limitations, in particular the masking of binding events that occurs in sample environments that have variant refractive indices. In cases where the molecules to be tested have been solubilised in organic solvents, or are components of a crude cell lysate, culture medium or a serum sample, optical based techniques often are incapable of measuring associated binding events without extensive calibration or sample preparation procedures. Thus, one notable advantage of acoustic detection over more established optical label-free detection is the relative insensitivity of acoustics to changes in solvent. When running samples containing DMSO, optical detection systems suffer from large bulk refractive index shifts that arise from the disparate properties of the organic solvent and the running buffer. For example, the dielectric constant of water is 80, whereas for DMSO it is 40 (a difference of 100%). To normalise for these large bulk effects, a calibration routine using known serial dilutions of DMSO in running buffer is normally run a the beginning, middle and end of a screening panel [65]. In contrast, acoustic systems are not effected by refractive index changes, but are instead sensitive to bulk effects dominated by viscosity and density of the solvent; more specifically the square root of the viscosity:density product [14]. For water, this value is 0.99, whereas for DMSO it is 1.10 (a difference of only 11%).

1.11 Theoretical Considerations

The possibility of using quartz crystal resonators as quantitative mass measuring devices was first explored by Sauerbrey. The decrease of the resonant frequency of a thickness shear vibrating quartz crystal resonator, having AT or BT cut, was found to be proportional to the added mass of the deposited film. The derivations of Kanazawa and others when one face of a quartz crystal resonator is in contact with a liquid, and the calculation of penetration depth is dealt with elsewhere in this volume. Brown et al. [66] have attempted to extend the theory to accommodate polymeric or other finite viscoelastic layers acoustically coupled to the rigid quartz crystal and a rigid "ideal mass layer". This situation is analogous to a biological receptor layer coupled covalently to a rigid, high shear modulus chemical linker layer (Fig. 8). Brown

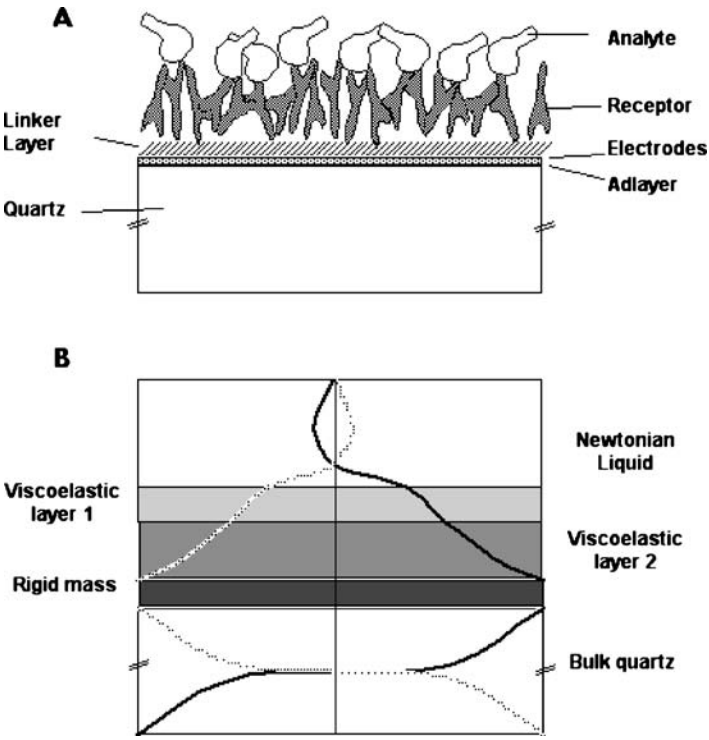

Fig. 8 Idealised model of acoustic attenuation. **A** Diagrammatic representation of a thickness shear mode bulk acoustic wave resonator, coated with a rigid metal adhesion and electrode layer, a rigid chemical linker layer, a finite viscoelastic antibody receptor layer, a second adherent finite viscoelastic analyte layer, and finally a Newtonian liquid. **B** An idealised model of acoustic attenuation from bulk quartz through the above layers of varying viscosity, density, and shear modulus

et al. considered a finite viscoelastic layer (of thickness h_f, density r_f and shear modulus $G = G' + jG''$. The latter value, G, is the complex shear modulus where G' and G'' are the layer storage and layer loss moduli respectively.

These layers are then exposed to a bulk liquid (of viscosity η_L and density ρ_L) (Fig. 8). For these layered components, it is possible to derive the surface mechanical impedances:

$$Z_M = j\omega\rho_s \tag{4}$$

for the ideal/rigid mass layer (in Akubio's the chemical linker layer), where r_s is the mass per area contributed by the linker layer:

$$Z_F = \sqrt{\rho_f G}\tan h(\gamma h_f) \tag{5}$$

for the viscoelastic film (biological film), where γ is the shear wave propagation constant ($\gamma = j2\pi f_0(r_f)^{1/2}$) and $j = \sqrt{-1}$:

$$Z_L = \sqrt{\frac{2\pi f_o \rho_L \eta_L}{2}}(1 + j), \tag{6}$$

for the liquid layer (semi-infinite Newtonian liquid), and finally:

$$Z = j2\pi f_o \sqrt{\rho_f G}\frac{Z_L \cos h(\gamma h_f) + \sqrt{\rho_f G}\sin h(\gamma h_f)}{\sqrt{\rho_f G}\cos h(\gamma h_f) + Z_L \sin h(\gamma h_f)}, \tag{7}$$

where Z is the impedance for the composite system. Note that the impedance measured by the resonator is *not* simply the sum of those for individual layers, as for each layer there will be an acoustic phase shift, which causes a transformation of the impedance contributed by layers more distant from the resonator. In addition this model does not accommodate the typically inhomogeneous layers that exist in reality in biological systems (e.g. a hydrated protein layer), or changes in distribution of mass induced by varying matrix conditions and analyte binding.

When layers of a material of differing density and viscosity to the liquid (such as a protein film) are deposited at the surface–liquid interface, then there is a contribution from both the bulk liquid and from the added material that has displaced liquid and mechanically coupled to the interface. In this case the penetration depth can be defined as:

$$\delta = (1 - \chi_p)\sqrt{\frac{\eta_L}{\pi f_o \rho_L}} + \chi_p \sqrt{\frac{\eta_L}{\pi f_o \rho_f}}, \tag{8}$$

where η_p and ρ_p are the liquid viscosity and density, respectively, and χ_p is the fraction of the volume within the penetration depth occupied by protein. This could be extended to encompass both a receptor layer and analyte layer as shown in Fig. 8 if necessary. Integrating the mole fraction of protein/water in combination with the definition of a composite impedance (Eq. 7), we can

derive:

$$Z = \chi_p j 2\pi f_o \sqrt{\rho_f G} \frac{(1-\chi_p) Z_L \cos h(\gamma h_f) + \sqrt{\rho_f G} \sin h(\gamma h_f)}{\sqrt{\rho_f G} \cos h(\gamma h_f) + (1-\chi_p) Z_L \sin h(\gamma h_f)}. \quad (9)$$

In the case of a resonator coated with a linker chemistry, we can thus model a rigid (high shear modulus) linker layer with a coupled viscoelastic receptor layer, followed by binding of a viscoelastic analyte. The latter interaction is the most difficult to model as the impedance matching and acoustic transmission of the penetrative wave between the receptor layer and analyte layer will depend not only on the density, viscosity and shear modulus of the binding analyte, but also on the affinity of the interaction (van der Waals interactions, hydrogen bonds, induced dipole interactions etc. etc.), and conformational changes in the receptor that may be induced by analyte binding. Fortunately, pure mass responses can be calculated in buffered solutions via SPR measurements, whilst layer thickness can be determined by a combination of dry film ellipsometry measurements and hydrated liquid phase dual polarisation interferometer measurements. In addition, the contribution of viscosity and density to the acoustic load can be deconvoluted via measurement in varying concentrations of buffered glycerol in which the buffer is constituted from H_2O, or from D_2O.

1.12 Current and Future Applications of RAP™

Any system that utilises a highly sensitive transducer such as piezoelectric quartz to measure molecular interactions must possess a variety of integrated technical controls to facilitate the highest level of sensitivity, accuracy and precision. Previous attempts to exploit this detection method in a commercial format have been limited by poor sample delivery mechanics, inadequate thermal controls, and the lack of a multisensor analysis platform. The development of proprietary electronics, fitting algorithms and a low-stress mounting system for the sensor has enabled Akubio to integrate microfluidic delivery together with automated liquid handling in the RAP♦*id* system. Ease of use is further facilitated by a number of simple-to-use coupling chemistries for attachment of target proteins to the sensor surface, and flow-chart-based assay design software.

These features, together with the ability to directly analyse samples in crude matrices means RAP♦*id* could be a useful tool for the protein therapeutic and antibody engineering sectors. RAP♦*id* can directly determine active antibody concentration, interaction specificity, cross reactivity, affinity and dissociation rates/half lives during the early stage development of drug candidates. Later in the pipeline, the technology can also be applied to a fuller kinetic characterisation of the products and interactions with the therapeutic targets and side-effect profilers. The technology may also be applicable in

downstream manufacturing processes where the quantification of production and purification yields in a timely and accurate manor is critical.

In the past, acoustic detection has been used to characterise interactions with peptides [67, 68], proteins and immunoassay markers [16, 17, 19, 20], oligonucleotides [54, 55], bacteriophage [57, 69], viruses [70, 71], bacteria [36, 38, 39] and cells [43–46, 50, 51]. The technology can thus be applied to an extremely wide range of biological and chemical entities. This suggests that one of the most promising applications may be acoustic cell-based screening in which live cells or cell membrane fragments form an active part of the sensor. This would potentially enable pathway-based screens to be carried out on cells to identify or confirm modulators of disease pathways, then mode-of-action assays to be performed with purified receptors; both with a same label-free technique.

2 Rupture Event Scanning

The analysis of molecular interactions is an integral part of many processes in the fields of diagnosis, life sciences and drug discovery. Diagnostic and pharmaceutical companies spend many millions of dollars to screen compounds for receptor binding in vitro during the initial phase of the development of new drugs, and to screen for pathogens which cause human, animal and plant diseases. Rapid diagnosis of bacterial and viral infections is of paramount importance for disease prognosis and prompt administration of appropriate therapy. It is also important to accurately monitor bacterial and viral load in order to determine the efficacy of drug treatment. Traditional methods of diagnosis involve direct culture techniques that are time-consuming, prone to problems of contamination, and may take days or weeks to give a result. Immunoassays such as antibody ELISA are more rapid, but have limited sensitivity and generally are used only to detect the antibodies produced following infection, rather than the infectious agent itself. Oligonucleotide-based assays, which detect pathogenic DNA or RNA, are very sensitive, but are expensive and require considerable experimental skill, as the genetic material must be isolated before nucleic acid amplification [72]. These methods can provide valuable early results in some situations, but in many cases local facilities are not available and specimens are often transported to central reference laboratories for testing. Hence, there is a real need for methods that rapidly detect and identify pathogens, especially those organisms that cause life-threatening infections such as meningitis and septicaemia.

The majority of molecular screening in diagnosis, drug discovery and the life sciences is carried out by interrogating a sample with some form of electromagnetic radiation: radio waves, microwaves, infrared, visible light, ultraviolet light, X-rays or gamma radiation. The most widely utilised screens

require some type of radio or fluorescent labelling to report the binding of a ligand to its receptor. This labelling step imposes additional time and cost demands, and can in some cases interfere with the molecular interaction by occluding a binding site, leading to false negatives. Fluorescent compounds are invariably hydrophobic and in many screens background binding is a significant problem, leading to false positives. Ideally a screen should be universally applicable, label-free, sensitive, economical and rapid.

We have developed a new method of detecting analytes, which we term rupture event scanning or REVS™ [73]. The technology enables rapid, label-free determination of interaction affinities, both in buffered solutions *and* in complex biological fluids. Potential applications range from the diagnosis of clinical infections to the screening of libraries for receptor binding and the quantitation of molecular interactions in general. The detection technology does not utilise any form of electromagnetic radiation, but instead records vibrational excitation in a substrate caused by disruption of molecular interactions. To induce a molecular complex of moderate affinity to break apart requires accelerations many orders of magnitude higher than the forces due to gravity. These very high forces can be imparted on an analyte by using an acoustic wave device, such as a quartz crystal resonator. In contrast to other quartz crystal biosensing applications (quartz crystal microbalance or quartz crystal resonance sensing), REVS™ technology does not only use the quartz resonator as a sensor, but takes advantage of the active surface of the resonator and its influence on systems adhered to it. However, REVS™ technology and our experimental set-up are also compatible with standard frequency and resistance shift measurements [74–76]. By monitoring the change in resonant frequency and resistance of the crystal, which occur upon adsorption of analytes to the surface, quartz crystal resonators can be used together with appropriate surface chemistry and fluidics to detect the adsorption of proteins, oligonucleotides, cells and other analytes to surface-bound receptors [77]. This allows the label-free determination of interaction affinities and kinetics in real time. In this short review the capabilities of REVS™ detection will be demonstrated using the herpes simplex virus as a model system.

2.1 Controlled Applied Force

As the magnitude of an applied electric field applied to a piezoelectric material is increased, the amplitude of oscillation increases and there is increasing acceleration of analytes adhered to the surface. This in turn results in an increasing force exerted by the surface on the analytes, which ultimately causes rupture of the bonds attaching the analytes to the surface (Fig. 9). Due to its piezoelectric properties the quartz crystal can be used to detect the excitation of vibrations in the substrate produced by bond rupture, which are converted into an electrical signal. The signal indicates not only the pres-

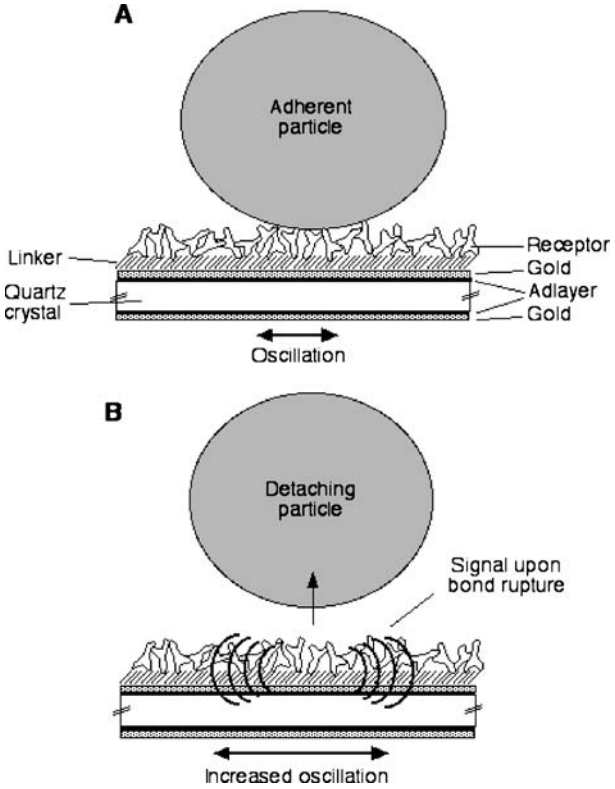

Fig. 9 REVS™ assay. **A** An AT-cut quartz crystal was coated successively with a chromium layer, a gold layer, a chemical linker layer, and a receptor that mediated specific attachment of the particle. The crystal was then transversely oscillated by applying a RF voltage at the main resonant frequency to the gold electrodes on either side of the disc. **B** Increasing the applied voltage results in a transverse oscillation of greater amplitude which, in principle, leads to greater inertial forces between the particle and the surface and concomitant deformation of the surface and the particle. Ultimately the bond between particle and receptor surface breaks and vibrations in the quartz are excited. These vibrations can be detected by using the quartz as a sensitive microphone. Note that the figures are not to scale

ence of the analytes but also the number of analytes present and their affinity for a surface-bound receptor. The scanning process requires minimal sample preparation, works well in buffered solutions *and* in complex biological fluids such as serum, and takes only minutes to perform.

The magnitude of excited vibrations is proportional to the number of analytes present over at least six orders of magnitude, right down to the level of a single particle, with a weight of only 80 fg, in 1 μL of fluid. This corresponds to a mass sensitivity of 80 fg mm^{-2} (8×10^{-14} g mm^{-2}) [73]. In comparison, traditional frequency change quartz crystal biosensors have a detection

limit in the order of 1 ng mm^{-2} (10^{-9} g mm^{-2}), whilst the best surface plasmon resonance optical biosensors can detect a mass change of 1 pg mm^{-2} (10^{-12} g mm^{-2}). The latter technique does not work well in complex fluids such as undiluted serum, as there is significant non-specific binding of materials such as serum proteins to the sensor surface.

The resonators used for REVS™ are commercially available polished AT-cut quartz discs with a diameter of 8.25 mm and a main resonant frequency at 14.3 MHz. The electrodes consist of a 3 nm thin chromium adhesion layer and between 40–80 nm of evaporated gold. The gold electrodes are covered with a chemical linker layer to which the desired receptors are attached. A signal generator is used to drive the quartz crystal at its fundamental resonant frequency, or at a higher overtone. During one scan the drive level is increased from 0 to 10 V. The response of the quartz at three times the fundamental frequency is fed via a filter into a lock-in amplifier and analysed using a signal generated by a second amplifier as reference. A more detailed description can be found in reference [78].

2.2 Detection of Herpes Simplex Virus

Rupture event scanning is a useful addition to existing techniques, as it combines the specificity and versatility of ELISA with the sensitivity of PCR [79]. The ability to include antibodies as a capture reagent adds a critical advantage to the technique, as it can build on the wide availability and tremendous knowledge base of monoclonal antibodies against viruses and bacteria [80]. The application of REVS™ for viral diagnosis has been validated with herpes simplex virus (HSV), which causes recurrent mucosal infections of the eye, mouth and genital tract. It also causes life-threatening generalised infection in the new-born and, more rarely, a fatal encephalitis in adults [81]. Rapid and sensitive detection of HSV is not a major public health issue except in the case of herpes encephalitis, where rapid detection of virus particles in cerebrospinal fluid is a prerequisite for appropriate chemotherapy. HSV is, however, a relatively fragile enveloped virus particle, sensitive to heat and desiccation, and is therefore a reasonable surrogate for many viruses of clinical importance such as HIV, hepatitis viruses B and C, and influenza.

For specific detection of HSV the viral samples were incubated for 40 min on the antibody-coated quartz crystals, washed with phosphate buffered saline solution (PBS) and then scanned under PBS from 0–10 V. A sharp peak at approximately 7.4 V with a signal strength of 450 arbitrary units was detected for a surface coated with HSV specific antibodies, whereas no signal was detected on surfaces coated with antibodies to which HSV does not bind (Fig. 10). This demonstrates that REVS™ only detects specifically bound viruses. A second scan of the driving voltage from 0–10 V immediately following the first gave no peaks, indicating that the viruses had been

detached from the surface. To confirm that the interaction between virus and surface was specific, control experiments were carried out using a modified herpes simplex virus missing the protein to bind to the antibody on the surface. The interaction was also specifically blocked by pre-incubating the

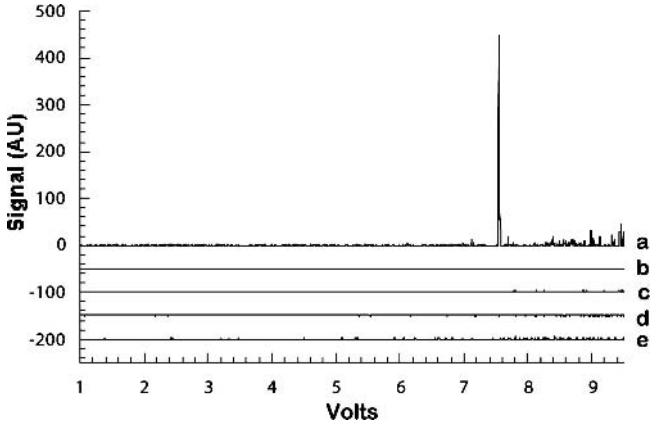

Fig. 10 Herpes simplex virus detection. Validation for specific detection of herpes simplex virus using REVS™: **a** 500 000 HSV (gD^+) virions incubated on a surface coated with an HSV receptor (anti-gD monoclonal antibody), **b** the same number of HSV virions on a surface with a receptor to which HSV does not bind (control bovine IgG), **c** genetically modified HSV (gD^-) on HSV receptor surface, **d** HSV on a soluble gD-blocked HSV receptor surface, **e** HSV in blocking solution (anti-gD monoclonal antibody) on HSV receptor surface. The traces have been displaced from zero on the y-axis for clarity

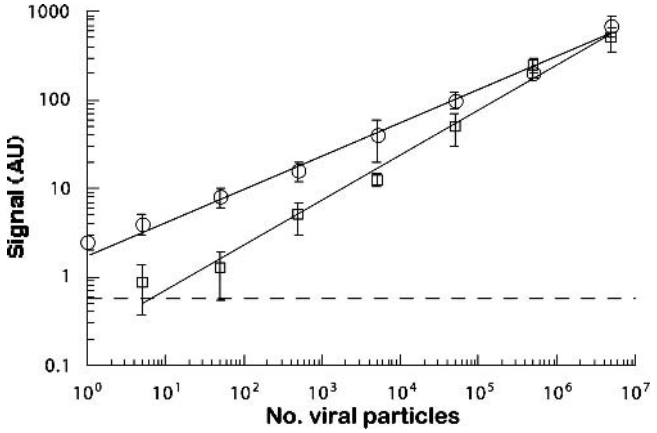

Fig. 11 Limits of detection for REVS™. Signal linearity with particle numbers. Serial tenfold dilutions of HSV1 gD^+ in PBS a sample volume of either 1 μL (*open circle*) or 40 μL (*open squares*) incubated for 40 min at room temperature on a quartz crystal coated with an HSV specific antibody. The *dashed line* represents the noise floor

antibody surface with the protein responsible for HSV binding (surface blocking) and by using HSV pre-incubated with antibodies before deposition on the antibody-covered quartz surface (solution blocking). In all cases no signal was observed (Fig. 11), confirming that REVS™ is an accurate method to detect specifically bound analytes.

To determine the sensitivity limits of detection, a HSV sample was serially diluted in phosphate buffered saline solution. The REVS™ signal specific for detachment of HSV was log-linear with the number of viruses over six orders of magnitude using a 1 μL sample (Fig. 11). The signal intensity using a 40 μL sample volume was approximately fivefold lower than that obtained using a 1 μL sample. This is believed to be due to a slower diffusion of virions to the surface in the larger sample volume, which results in a lower amount of captured virus on the sensor surface when the same incubation period is used with the larger sample volumes.

2.3 Theory

REVS™ is a novel detection and measurement method very different to classical quartz crystal resonant sensing (QCRS), which typically involves measurement of changes in frequency and resistance of the resonator. Whereas in QCRS the resonator is a passive transducer of binding events at the solution–surface interface, in REVS™ the resonator plays an active role in forcing bond rupture and then also detecting modulations in the resonance of the crystal induced by this event. Whilst we have a basic understanding of the processes involved in REVS™, we acknowledge that much more experimental and theoretical work is needed to fully understand the nature of the detachment event and signal generation. Long- and short-range interactions between molecules are central to the dynamic behaviour of biological systems. These interactions have traditionally been examined in great detail using thermodynamic approaches. However, the rupture of these interactions is a dynamic process and it is well known that the force required to break bonds depends not only on the affinity of the interactions, but also on the rate at which the force is applied to the interacting molecules [82, 83]. In recent years a variety of instruments have been developed to measure the force between molecules, including glass fibres, optical tweezers, the surface force apparatus and the atomic force microscope (AFM). Of these, the AFM has rapidly become one of the most widely used force measurement instruments due to its ease of use and its commercial availability [84]. AFM measurements are, however, most often carried out on single molecule interactions in which a single bond between two binding partners is broken. REVS™ possesses single molecule sensitivity, however, many of the analytes studied to date (such as viruses and bacteria) present multiple bonds to the surface of the resonator. It is also notable that a discrete, transient signal is observed from detachment events

involving large number of surface-bound analytes. For example, Fig. 9a shows a sharp peak for the detachment of 500 000 virions. These particles possess slightly varying shapes, sizes and, in particular, different numbers of bonds to receptors on the surface. Nevertheless, they dissociate from the surface of the resonator in a very short period giving rise to the high signal to noise peaks observed with REVS™.

For the purposes of this discussion we will assume that, up to the threshold rupture voltage, adherent particles are mechanically coupled to receptors on the surface via short-range molecular forces (i.e. electrostatic, hydrophobic, ion-dipole, Van der Waals interactions etc.). Transient forces due to inherent thermal energy of the bound complexes are by themselves insufficient to break multiple bonds in the short (1 min) assay time of a REVS™ scan; a necessary condition for subsequent dissociation of the particle. In other words, it is highly improbable that multiple antibody–antigen bonds will all rupture simultaneously at room temperature. It should also be noted that biomolecules such as proteins and viruses are stabilised by weak interactions (for example, the free enthalpies for binding of typical antibody–antigen interactions are in the order of $\sim 50\,\mathrm{kJ\,mol^{-}1}$ [85], with detachment forces measured by AFM in the order of 10–200 pN [86, 87]).

Under the force loading on crystal experienced at high driving voltages, some of the bonds between virus and the antibody on the surface of the resonator will be ruptured, and the particle may partially decouple from the surface of the crystal. The resulting increased force on the remaining intact bonds could then lead to an increased rupture rate of the remaining bonds. This positive feedback mechanism can potentially explain the transient characteristic of REVS™ peaks. This is an attractive hypothesis; however, it is also important to consider the case in which the load on the particle may be wholly, or partially, concentrated on one bond at a time, in which case the bonds will rupture in series [87]. It is also possible that the bonds can reform within the timescale of the rupture event.

To calculate the forces imparted on a molecule on the surface of the resonator it is first necessary to determine the displacement amplitude of the resonator. This has been shown to depend linearly on the merit factor and the drive level. For an AT cut quartz resonator it can be calculated from the following relationship:

$$A = 1.4\ Q\ V_{\mathrm{d}}\,, \tag{10}$$

where A is the amplitude of maximal displacement of the thickness shear mode resonator, the factor of 1.4 (pm V^{-1}) is a proportionality constant determined by Borovsky et al. [88], Q is merit factor of the resonator and V_{d} is the driving voltage. Note that this measured proportionality constant is the same as that calculated theoretically by Kanazawa [14]. Within Kanazawa's model the amplitude is interpreted as the average amplitude across the crystal surface. This is expected to be about one half the maximum amplitude

at the centre of the crystal, in view of the approximately Gaussian amplitude distribution [14, 88]. The Q factor in our experiments under liquid has been determined to be 1400–1600, depending on the resonator used. For a driving voltage of 7 V this gives an estimated vibrational amplitude at the centre of the crystal of ~ 15 nm.

If we assume that particles detected using REVS™ are spherical and attached at a point to the surface of the resonator, we can determine the ratio between force applied tangentially to the surface of the particle and acceleration of the surface of the particle. We also assume that sphere is rolling, or pivoting about this attachment point, which we acknowledge is an approximation of the geometry of the virus–antibody interaction. The moment of inertia of the sphere about a central axis, J_s is defined as:

$$J_s = \int r^2 \mathrm{d}m = 2\pi\rho \int_0^{R_s} r^4 \left(\sqrt{R_s - r^2}\right) \mathrm{d}r = \frac{2}{5} M_s R_s^2 , \tag{11}$$

where r is the integrated radius, R_s is the radius of the sphere, M_s is the mass of the sphere, and ρ is the density of the sphere. The acceleration at the centre of the sphere, a_c is defined as:

$$a_c = \frac{F_t}{M_s} , \tag{12}$$

where F_t is applied total force. The angular acceleration ε_s of the sphere is thus defined as:

$$\varepsilon_s = \frac{F_t R_s}{J_s} = \frac{F_t R_s}{\frac{2}{5} M_s R_s^2} = \frac{5 a_c}{2 R_s} , \tag{13}$$

which makes acceleration of surface of the sphere, a_s with respect the acceleration at its centre, a_c:

$$a_s = \varepsilon_s R_s = \frac{5 a_c}{2} , \tag{14}$$

and hence the total acceleration of the surface of the sphere, a_{ts} is:

$$a_{ts} = a_c + a_s = a_c + \frac{5 a_c}{2} = \frac{7 a_c}{2} . \tag{15}$$

In other words, for a sphere pivoting about an attachment point to a surface, the centre of mass of the sphere moves only 2/7th of the distance moved by the surface at full amplitude about the pivot point. The acceleration of a point on the surface of the resonator thus is given as:

$$a = \frac{2}{7} A (2\pi f)^2 . \tag{16}$$

For the 14.2 MHz crystals driven at 7 V employed in our work this gives an acceleration on the surface of 3.4×10^7 m s^{-2} or 3.4 million g! We can estimate the mass of a single virus from knowledge of its molecular weight

($\sim 5 \times 10^8$ Da) which gives the mass of a single virion as 80 fg [81, 89]. Ignoring any contribution from viscous forces in water and treating the virion as a rigid sphere, this then enables us to estimate the force imparted on a virion adhered to the resonator from:

$$F = \frac{2}{7} mA(2\pi f)^2 \tag{17}$$

giving F as ~ 3 nN. This raises the question: is this force sufficient to break bonds typically found in biological systems? Atomic force microscopy has been used to determine the forces involved in single molecule interactions between antibodies and antigens immobilised on planar surfaces, with typical measured values in the order of 10–200 pN [86, 87]. However, the virus used in this study presents multiple receptors on its surface, and will form multiple bonds with several antibodies on the surface of the resonator. Indeed, adhesion to surface-bound receptors in biology is characterised by polyvalent interactions and multiple receptor–ligand interactions, which serve to enhance the affinity, or avidity of an interaction. To determine exactly the number of interacting molecules during each measurement a prior knowledge of the surface density of the immobilised molecules, particle geometry and particle–receptor contact area is required. Surface coverage can be estimated using radio-labelling and fluorescence techniques. However, determination of particle and receptor orientation and the contact area between the two is problematical, and we have not taken this into account in our calculations. It has also been demonstrated that there is a strong dependence in the measured adhesion force between biomolecules and the loading rate (or pulling rate in the case of AFM) [85, 90]. Notwithstanding these effects, it can clearly be seen that the force imparted by the resonator on the adherent virion (3 nN), is sufficient to rupture several bonds between the particle and receptors immobilised on the surface (10–200 pN each).

2.4 Application to Model Clinical Samples

For REVS™ applications using clinical samples, it is necessary to detect viruses in more complex biological fluids, such as serum or cerebrospinal fluid, which contain large quantities of proteins. To test the suitability of the REVS™ technique for use in complex specimens, HSV samples were diluted in calf serum. Peaks were observed in the region of 7.1 V (Fig. 12). The fact that multiple, distinct peaks can be observed in serum may be due to partial non-specific blocking of some antibody binding sites by serum proteins, which could lead to more variations in the number of interactions between the virus and the surface than is the case in PBS.

These results demonstrate that REVS™ technology could potentially be applied to a wide range of more complex biological samples. Quartz crystal

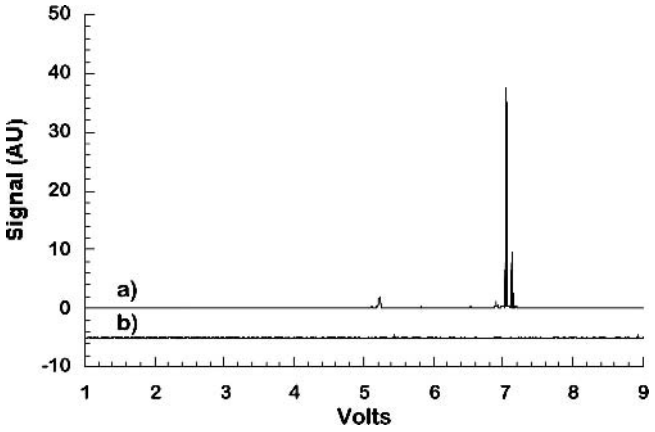

Fig. 12 Detection in neat serum. **a** 1 μL of HSV gD^+ at 5×10^7 particles/mL in calf serum incubated for 40 min on a quartz resonator coated with anti-gD IgG monoclonal antibody, then washed with water and scanned under 10 μL of PBS from 0–10 V. **b** Calf serum only incubated for 40 min on a QCM disc coated with anti-gD IgG monoclonal antibody, then washed with water and scanned under 10 μL of PBS from 0–10 V

resonators have been mass-produced for many years and are relatively inexpensive. The oscillation and detection system is entirely electronic, which results in a direct digital read out without the use of optics, filters, charge-coupled devices or image processing. This makes the instrumentation much simpler and cheaper than is the case with fluorescence, chemiluminescence or evanescent wave-based techniques. The major challenges that lie ahead include the successful integration of the detection technology with fluidics, chemistry, biology, signal processing, and data management. It is possible to multiplex the assay in a variety of ways and also to miniaturise the detector for direct detection in the field or at patient point of care. The label-free nature of the technique should allow rapid assay development with broad applicability to the detection of viruses, bacteria, cells, proteins, oligonucleotides and small molecules. Akubio's acoustic detection technology thus has great potential as a new method for interrogating chemical and biological samples in drug discovery, diagnosis, and the life sciences in general.

Acknowledgements The author wishes to thank all the employees, cofounders and consultants of Akubio Ltd.

References

1. Myszka DG, Jonsen MD, Graves BJ (1998) Anal Biochem 265:326
2. Myszka DG, Rich RL (2000) Pharm Sci Tech Today 3:310
3. Cooper MA (2002) Nature Reviews Drug Discovery 1:515
4. Rich RL, Myszka DG (2005) J Mol Recognit 18:1

5. Curie P, Curie J (1880) C R Acad Sci 91:294
6. Nomura T, Okuhara M (1982) Anal Chim Acta 142:281
7. Auge J, Hauptmann P, Hartmann J, Rosler S, Lucklum R (1995) Sensor Actuator B-Chem 24:43
8. Marx KA, Zhou TA, Montrone A, Schulze H, Braunhut SJ (2001) Biosens Bioelectron 16:773
9. Thompson M, Hayward GL (1997) Proc IEEE Int Freq Control Symp, p 114
10. Ghafouri S, Thompson M (2000) Electroanalysis 12:326
11. Hayward GL, Thompson M (1998) J Appl Phys 83:2194
12. Theisen LA, Martin SJ, Hillman AR (2004) Anal Chem 76:796
13. Arnau A, Jimenez Y, Sogorb T (2001) IEEE T Ultrason Ferr 48:1367
14. Kanazawa KK (1997) Faraday Discuss, p 77
15. Geelhood SJ, Frank CW, Kanazawa K (2002) J Electrochem Soc 149:H33
16. Aizawa H, Kurosawa S, Ogawa K, Yoshimoto M, Miyake J, Tanaka H (2001) Sensor Actuator B-Chem 76:173
17. BenDov I, Willner I, Zisman E (1997) Anal Chem 69:3506
18. Ghourchian HO, Kamo N (1995) Anal Chim Acta 300:99
19. Kurosawa S, Aizawa H, Yoshimoto M (2000) IEEE T Ultrason Ferr 47:1256
20. Percival CJ, Stanley S, Braithwaite A, Newton MI, McHale G (2002) Analyst 127:1024
21. Wu ZY, Shen GL, Xie LJ, Yu RQ (2000) Sensor Actuator B-Chem 71:99
22. Suleiman AA, Guilbault GG (1991) Anal Lett 24:1283
23. Uttenthaler E, Kosslinger C, Drost S (1998) Biosens Bioelectron 13:1279
24. Wang H, Lei CX, Li JS, Wu ZY, Shen GL, Yu RQ (2004) Biosens Bioelectron 19:701
25. Aizawa H, Kurosawa S, Tanaka M, Wakida S, Talib ZA, Park JW, Yoshimoto M, Muratsugu M, Hilborn J, Miyake J, Tanaka H (2001) Mater Sci Eng C-Biomimet Supramol Sys 17:127
26. Hu JM, Pei RJ, Hu Y, Zeng YE (1998) Chinese J Chem 16:219
27. Su XD, Chew FT, Li SFY (2000) Biosens Bioelectron 15:629
28. Aizawa H, Kurosawa S, Tozuka M, Park JW, Kobayashi K, Tanakac H (2003) Biosens Bioelectron 18:765
29. Long YM, Li WF, Nie LH, Yao SZ (2001) J Pharmaceut Biomed 24:361
30. Su XD, Chew FT, Li SFY (1999) Anal Biochem 273:66
31. Bao L, Deng L, Nie L, Yao S, Wei W (1996) Anal Chim Acta 319:97
32. Minunni M, Mascini M, Carter RM, Jacobs MB, Lubrano GJ, Guilbault GG (1996) Anal Chim Acta 325:169
33. Ye JM, Letcher SV, Rand AG (1997) J Food Sci 62:1067
34. Park IS, Kim N (1998) Biosens Bioelectron 13:1091
35. Park IS, Kim WY, Kim N (2000) Biosens Bioelectron 15:167
36. Fung YS, Wong YY (2001) Anal Chem 73:5302
37. Aizawa H, Kurosawa S, Tanaka M, Yoshimoto M, Miyake J, Tanaka H (2001) Anal Chim Acta 437:167
38. Otto K, Elwing H, Hermansson M (1999) J Bacteriol 181:5210
39. Spangler BD, Wilkinson EA (2000) Abstracts of papers of the Am Chem Soc 219: U115
40. Wong YY, Ng SP, Ng MH, Si SH, Yao SZ, Fung YS (2002) Biosens Bioelectron 17:676
41. Pavey KD, Ali Z, Olliff CJ, Paul F (1999) J Pharm Biomed Anal 20:241
42. Pavey KD, Barnes LM, Hanlon GW, Olliff CJ, Ali Z, Paul F (2001) Lett Appl Microbiol 33:344
43. Richert L, Lavalle P, Vautier D, Senger B, Stoltz JF, Schaaf P, Voegel JC, Picart C (2002) Biomacromolecules 3:1170

44. Rodahl M, Hook F, Fredriksson C, Keller CA, Krozer A, Brzezinski P, Voinova M, Kasemo B (1997) Faraday Discuss p 229
45. Fredriksson C, Kihlman S, Rodahl M, Kasemo B (1998) Langmuir 14:248
46. Shinohara H (1999) Electrochemistry 67:280
47. Ebato H, Okahata Y, Matsuda T (1993) Kobunshi Ronbunshu 50:463
48. Gryte DM, Ward MD, Hu WS (1993) Biotechnol Progr 9:105
49. Ebersole RC, Foss RP, Ward MD (1991) Bio-Technology 9:450
50. Braunhut SJ, Marx KA, Zhou T, Warren MC, Schulze HM (1999) Mol Biol Cell 10:64a
51. Wegener J, Seebach J, Janshoff A, Galla HJ (2000) Biophys J 78:2821
52. Mannelli I, Minunni M, Tombelli S, Mascini M (2003) Biosens Bioelectron 18:129
53. Minunni M, Tombelli S, Mariotti E, Mascini M (2001) Fresenius J Anal Chem 369:589
54. Caruso F, Furlong DN, Niikura K, Okahata Y (1998) Colloids Surf B-Biointerfaces 10:199
55. Hook F, Ray A, Norden B, Kasemo B (2001) Langmuir 17:8305
56. Caruso F, Rodda E, Furlong DF, Niikura K, Okahata Y (1997) Anal Chem 69:2043
57. Uttenthaler E, Schraml M, Mandel J, Drost S (2001) Bios Bioelectron 16:735
58. Lahiri J, Isaacs L, Tien J, Whitesides GM (1999) Anal Chem 71:777
59. Sigal GB, Bamdad C, Barberis A, Strominger J, Whitesides GM (1996) Anal Chem 68:490
60. Ernst OP, Bieri C, Vogel H, Hofmann KP (2000) Meth Enzymol 315:471
61. Casey PE (2004) AACN Clin Issues 15:547
62. Gibson RM, Rothwell NJ, Le Feuvre RA (2004) Vet J 168:230
63. Silva-Mejias C, Gamboa-Antinolo F, Lopez-Cortes LF, Cruz-Ruiz M, Pachon J (1995) Chest 108:942
64. Reimund JM, Wittersheim C, Dumont S, Muller CD, Kenney JS, Baumann R, Poindron P, Duclos B (1996) Gut 39:684
65. Frostell-Karlsson A, Remaeus A, Roos H, Andersson K, Borg P, Hämäläinen M, Karlsson R (2000) J Med Chem 43:1986
66. Brown MJ, Hillman AR, Martin SJ, Cernosek RW, Bandey HL (2000) J Mater Chem 10:115
67. Furtado LM, Su HB, Thompson M, Mack DP, Hayward GL (1999) Anal Chem 71:1167
68. Thompson M, Su HB, McGovern M, Kwong K, Mack D (1997) Abstracts of papers of the Am Chem Soc 213:213
69. Hengerer A, Kosslinger C, Decker J, Hauck S, Queitsch I, Wolf H, Dubel S (1999) Biotechniques 26:956
70. Zhou XD, Liu LJ, Hu M, Wang LL, Hu JM (2002) J Pharmaceut Biomed 27:341
71. Susmel S, O'Sullivan CK, Guilbault GG (2000) Enzyme Microb Tech 27:639
72. Higuchi R, Fockler C, Dollinger G, Watson R (1993) Biotechnology (NY) 11:1026
73. Cooper MA, Dultsev FN, Minson T, Ostanin VP, Abell C, Klenerman D (2001) Nat Biotechnol 19:833
74. König B, Grätzel M (1994) Anal Chem 66:341
75. Ballantine DS, White RM, Martin SJ, Ricco AJ, Zellers ET, Frye GC, Wohltjen H (1997) Acoustic wave sensors. Academic, San Diego
76. Ward MD, Buttry DA (1990) Science 249:1000
77. Janshoff A, Galla H-J, Steinem C (2000) Angewandte Chemie 39:4004
78. Dultsev FN, Ostanin VP, Klenerman D (2000) Langmuir 16:5036
79. Saphire EO, Parren PW (2001) Nat Biotechnol 19:823
80. Parren PW, Burton DR (2001) Adv Immunol 77:195
81. Minson AC (1998) In: Mahy BWJ, Collier L (eds) Topley and Wilson's microbiology and microbial infections, vol 1. Arnold, London, p 325

82. Evans E (2001) Annu Rev Biophys Biomol Struct 30:105
83. Evans E (1998) Faraday Discuss, p 1
84. Heinz WF, Hoh JH (1999) Trends Biotech 17:143
85. Evans E, Ritchie K (1999) Biophys J 76:2439
86. Guttenberg Z, Bausch AR, Hu B, Bruinsma R, Moroder L, Sackmann E (2000) Langmuir 16:8984
87. Seifert U (2000) Phys Rev Lett 84:2750
88. Borovsky B, Mason BL, Krim J (2000) J Appl Phys 88:4017
89. Regenmortel MV, Fauquet C, Bishop DHL (2000) Virus taxonomy. Academic, London
90. Merkel R, Nassoy P, Leung A, Ritchie K, Evans E (1999) Nature 397:50